Supplemental: Handicap principle implies emergence of dimorphic ornaments

Sara M. Clifton,[1,*] Rosemary I. Braun,[2,3] and Daniel M. Abrams[1,3,4]

[1] *Department of Engineering Sciences and Applied Mathematics, Northwestern University, Evanston, Illinois 60208, USA*
[2] *Division of Biostatistics, Northwestern University, Chicago, Illinois 60611, USA*
[3] *Northwestern Institute for Complex Systems, Northwestern University, Evanston, Illinois 60208, USA*
[4] *Department of Physics and Astronomy, Northwestern University, Evanston, Illinois 60208, USA*

Proceedings of the Royal Society B, doi:10.1098/rspb.2016.1970

I. THE CONNECTION BETWEEN POTENTIAL AND FITNESS

Many evolutionary dynamics problems begin with the replicator equation [1], which in the continuum limit is as follows:

$$\frac{\partial p}{\partial t} = p(a,t)\left[f(a,p) - \bar{f}(p)\right], \tag{S1}$$

where p is the probability distribution of a continuous phenotype a at time t, f is the fitness of a phenotype (say, ornament size or brightness) given a population state, and $\bar{f} = \int_{-\infty}^{\infty} f(a,p)p(a,t)\,\mathrm{d}a$ is the average population fitness [2].

Given that probability must be conserved, the distribution of phenotypes must also follow the continuity equation

$$\frac{\partial p}{\partial t} = -\frac{\partial}{\partial a}\left(p\frac{\mathrm{d}a}{\mathrm{d}t}\right). \tag{S2}$$

This formulation differs from the replicator equation (S1) in that it requires specification of the phenotype flux $\mathrm{d}a/\mathrm{d}t$ rather than fitness f. Our approach treats this flux as derivable from some potential function, which we refer to as φ, the net "reproductive potential" (see equation (3)).

Intuitively, the relationship between our phenotype flux $\mathrm{d}a/\mathrm{d}t$ and the more commonly used replicator equation approach (the upward distribution flux) can be seen in figure S1. These reflect interchangeable ways of viewing the evolutionary process of optimising the probability distribution $p(a,t)$.

We can express the relationship between the two approaches mathematically simply by equating the right-hand-sides of equations (S1) and (S2), yielding

$$f - \bar{f} = -\frac{1}{p}\frac{\partial}{\partial a}\left(p\frac{\mathrm{d}a}{\mathrm{d}t}\right) = -c\left(\frac{1}{p}\frac{\partial p}{\partial a}\frac{\partial \varphi}{\partial a} + \frac{\partial^2 \varphi}{\partial a^2}\right) \tag{S3}$$

where the last equality makes use of equation (4). Integrating equation (S3) once with respect to a and using equation (4) yields an integro-differential equation for φ in terms of f:

$$\frac{\partial \varphi}{\partial a} = -\frac{1}{cp}\int_{-\infty}^{a} p\left(f - \bar{f}\right)\mathrm{d}a, \tag{S4}$$

assuming $p\,\mathrm{d}a/\mathrm{d}t \to 0$ as $a \to -\infty$.

II. FIXED POINTS FOR GENERAL CLASS OF POTENTIAL FUNCTIONS WITH MINIMUM OF 2 MORPHS

In our analysis of (5), we claim that "reasonable" potential functions lead to stratification from a nearly uniform population into multiple distinct morphs. Here we examine in more detail what we mean by "reasonable". Again we consider a potential function

$$\varphi = s\,\varphi^{(\mathrm{soc})} + (1-s)\,\varphi^{(\mathrm{ind})}, \quad s \in [0,1]$$

* E-mail me at: sclifton@u.northwestern.edu

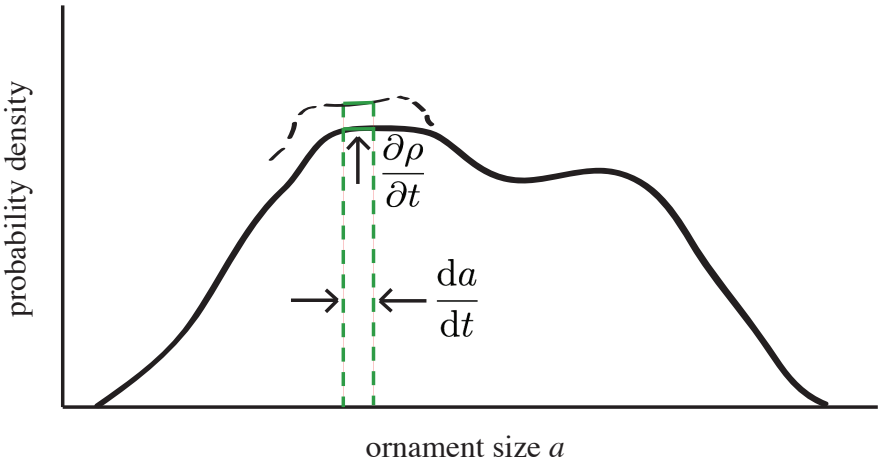

FIG. S1. (Colour online) Consider an infinitesimal sliver (dashed green) of the probability density function at a particular time (solid black). After an infinitesimal time increment, the probability density function changes a small amount (dashed black). Because probability is conserved, the flux $\mathrm{d}a/\mathrm{d}t$ of population ornament sizes into (or out of) the sliver increases (or decreases) the height of the probability density function.

where $\varphi^{(\mathrm{soc})}$ is a continuous and differentiable increasing function of ornament size, and $\varphi^{(\mathrm{ind})}$ is a continuous, singly-peaked function of ornament size. Assuming that the dynamics are such that ornaments grow on an evolutionary time scale at a rate proportional to marginal potential gain,

$$\frac{\mathrm{d}a}{\mathrm{d}t} \propto \frac{\partial}{\partial a}\varphi,$$

and we have $\dfrac{\mathrm{d}a}{\mathrm{d}t} = 0$ only for $a \geq a_{\mathrm{opt}}$.

We further assume that the following two criteria are satisfied:

1. Individual effects dominate reproductive potential for large ornament sizes. Specifically,

$$(1-s)\left|\frac{\partial}{\partial a}\varphi^{(\mathrm{ind})}\right| > s\left|\frac{\partial}{\partial a}\varphi^{(\mathrm{soc})}\right| \text{ as } a \to \infty. \tag{S5}$$

   This prevents ornament size from growing without bound, as can occur in equation (5) for $\gamma \geq 2$.

2. Social effects dominate reproductive potential for at least some range of ornament sizes greater than the population mean. In other words,

$$(1-s)\left|\frac{\partial}{\partial a}\varphi^{(\mathrm{ind})}\right| < s\left|\frac{\partial}{\partial a}\varphi^{(\mathrm{soc})}\right| \tag{S6}$$

   for at least some range of $a > \bar{a}$. Failure to meet this criterion could be considered "false" ornamentation, as can occur in equation (5) for $\gamma = 1$.

Assuming that the two-sided limits exist everywhere for both potential functions (a less strict requirement than continuity), these criteria guarantee that two or more morphs will emerge. See figure S2 (a)-(c) for graphical proof.

III. FIXED POINTS FOR GENERAL CLASS OF POTENTIAL FUNCTIONS WITH MAXIMUM OF 2 MORPHS

In our fixed points analysis of equation (5), we only consider uniform and two-morph steady states. We now show that these are the only types of fixed points for a wider class of potential functions, including our potential function (3). Consider a more general total potential function

$$\varphi = s\,\varphi^{(\mathrm{soc})} + (1-s)\,\varphi^{(\mathrm{ind})}, \quad s \in [0,1] \tag{S7}$$

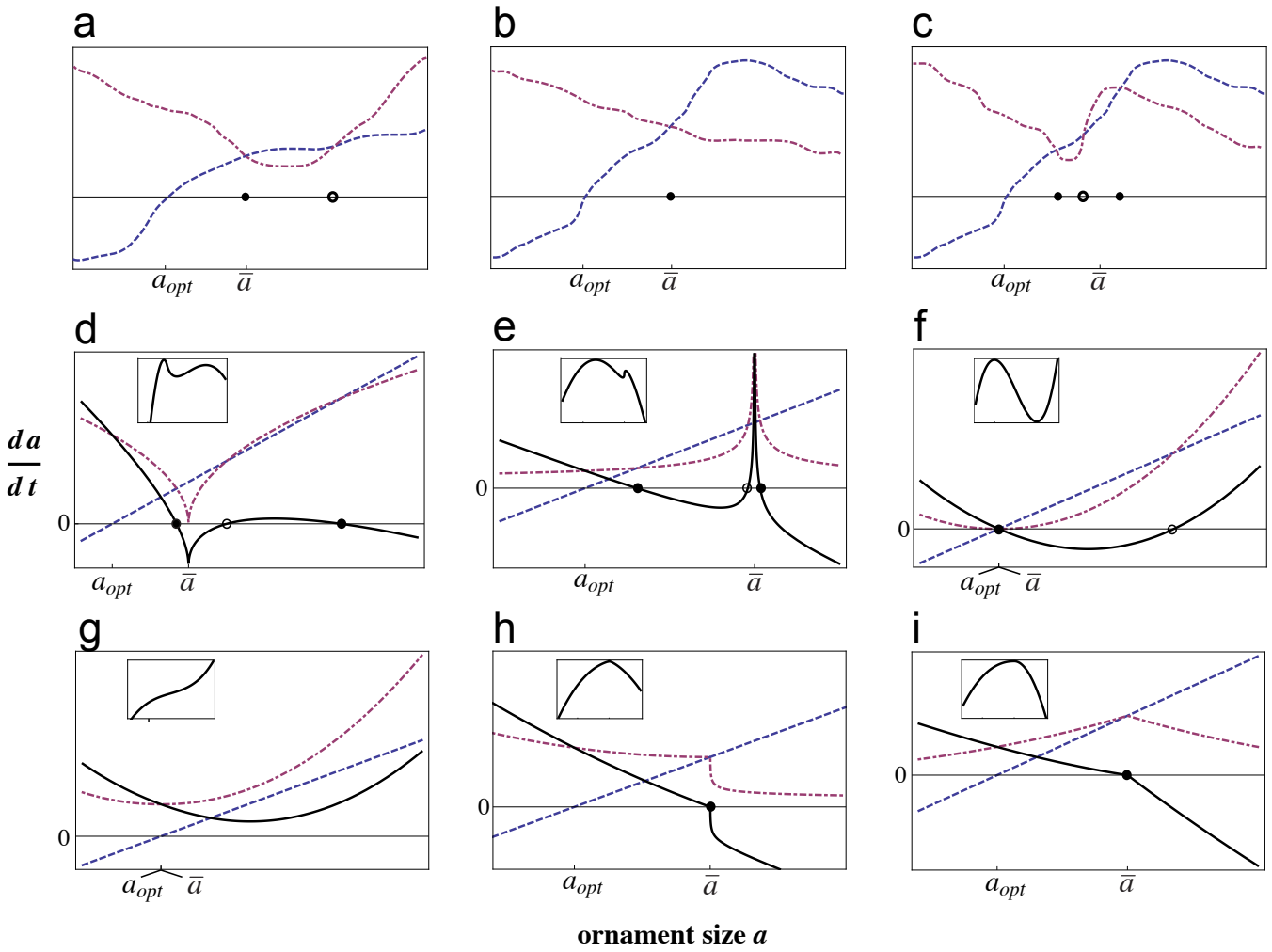

FIG. S2. (Colour online) Sketched examples of derivatives of negated individual potential (dashed blue) and social potential (dot dashed maroon) for a single male in a population near equilibrium. The derivative of total potential (solid black) is proportional to $\mathrm{d}a/\mathrm{d}t$, so intersections of individual and social potentials are the fixed points. Stable fixed points are marked with a filled black dot, and unstable fixed points are marked with an unfilled black dot. The total potential is inset. **(a)** An example of potential functions that satisfy restriction (S6), but not restriction (S5). In this case, both a stable uniform state and unbounded growth are possible. **(b)** An example of potential functions that satisfy restriction (S5), but not restriction (S6). In this case, the population will evolve to a uniform state. **(c)** An example of potential functions satisfying both restrictions (S5) and (S6). These conditions guarantee that the population will evolve into at least two morphs. **(d)-(i)** With restrictions (S8), the only possible stable steady states (filled black dots) are one- or two-morphs. Note that the system may or may not have an unstable node (unfilled black dots), or it may have no fixed points.

where $\varphi^{(\mathrm{soc})}$ is a continuous and differentiable increasing function of ornament size, and $\varphi^{(\mathrm{ind})}$ is a continuous, singly-peaked function of ornament size. Similar to our previous general class of potential functions,

$$\frac{\mathrm{d}a}{\mathrm{d}t} \propto \frac{\partial}{\partial a}\varphi,$$

we conclude that $\dfrac{\mathrm{d}a}{\mathrm{d}t} = 0$ only for $a \geq a_{\mathrm{opt}}$. This implies that equilibrium ornament sizes (if an equilibrium exists) will all be at least as large as the optimal. Because this is a first order ordinary differential equation model, we also know that oscillations are not possible.

We further assume that

$$\begin{aligned} &\frac{\partial^3}{\partial a^3}\varphi^{(\mathrm{ind})} \equiv 0 \\ &\frac{\partial^3}{\partial a^3}\varphi^{(\mathrm{soc})} > 0 \text{ or } \frac{\partial^3}{\partial a^3}\varphi^{(\mathrm{soc})} < 0, \quad a \neq \bar{a}. \end{aligned} \tag{S8}$$

In other words, individual potential is quadratic, and the derivative of social potential is either concave up or concave down, except possibly at the mean. With these additional restrictions on the potential function, only uniform and two-morph stable fixed points are possible. See figure S2 (d)-(i) for graphical proof. Our model (5) satisfies all restrictions, so we conclude that our exploration of the one- and two-morph steady states was a thorough investigation of all possible fixed points.

IV. CONTINUUM LIMIT

In the main manuscript, we derived the phenotype dynamics (5) of a system of N population representatives. The fixed points of this system are a discrete set of ornament sizes. Now we take $N \to \infty$, which turns the N ordinary differential equations into a partial integro-differential equation for a continuous distribution of ornament sizes $p(a,t)$. The equation we derive is the replicator function for continuous phenotypes [2].

We use conservation of probability to find the governing equation for the probability density function $p(a,t)$. The probability of a male having an ornament size in $(a, a+\mathrm{d}a)$ for small $\mathrm{d}a$ is approximately $p(a,t)\,\mathrm{d}a$. Given our assumption that individuals are neither created nor destroyed in $(a, a+\mathrm{d}a)$, we have

$$\frac{\partial p}{\partial t}\,\mathrm{d}a = p\,\frac{\mathrm{d}a}{\mathrm{d}t}\bigg|_{a} - p\,\frac{\mathrm{d}a}{\mathrm{d}t}\bigg|_{a+\mathrm{d}a}.$$

In other words, the change in individuals in the sliver $(a, a+\mathrm{d}a)$ is equal to the number that enter the sliver minus the number that leave. In the limit $\mathrm{d}a \to 0$, we get the continuity equation

$$\frac{\partial p}{\partial t} = -\frac{\partial}{\partial a}\left(p\,\frac{\mathrm{d}a}{\mathrm{d}t}\right). \tag{S9}$$

The dynamics of a follow (5) in the limit $N \to \infty$

$$\frac{\mathrm{d}a}{\mathrm{d}t} = c\Big[s\,\gamma|a-\bar{a}|^{\gamma-1} + 2(1-s)\,(a_{\mathrm{opt}} - a)\Big], \tag{S10}$$

where the mean ornament size is

$$\bar{a} = \int_{-\infty}^{\infty} a(t)\,p(a,t)\,\mathrm{d}a.$$

We substitute (S10) into (S2) to get a partial integro-differential equation for the probability density function $p(a,t)$ for ornament size

$$\frac{\partial p}{\partial t} = -c\frac{\partial}{\partial a}\left(p\left[s\,\gamma|a-\bar{a}|^{\gamma-1} + 2(1-s)\,(a_{\mathrm{opt}} - a)\right]\right). \tag{S11}$$

A. Continuum limit uniform steady state

Now that we have established the continuum limit of the discrete model, we wish to investigate the fixed points we found previously. Within this continuum framework, the uniform fixed point $a = a_{\mathrm{opt}}$ is the delta distribution

$$p(a,t) = \delta(a - a_{\mathrm{opt}}). \tag{S12}$$

Previously, we investigated the stability of the uniform steady state by perturbing every member of the population by the same arbitrary, small amount. If we wished to repeat this investigation for the continuum model, we would shift the peak of the delta function by an arbitrary small amount from a_{opt} to some a_0. To make stability analysis

more general, we also consider widening the delta function into a narrow Gaussian with an arbitrary small standard deviation σ. Figure S3 (a),(b) illustrate this idea.

We now wish to confirm that this continuum representation (S10) of the model is consistent with our discrete model (5), at least near the simplest fixed point (the uniform state). Based on our previous stability analysis, we expect that a_0 will shift back to a_{opt} and the width of the peak will shrink to 0 for $\gamma \geq 2$. However, we do not know how quickly these shifts occur relative to each other.

We will first investigate the dynamics of a_0 (i.e. σ is effectively constant on the time scale of interest). Then the "perturbed" distribution is the narrow Gaussian

$$p(a,t) = \frac{1}{\sigma\sqrt{2\pi}} e^{-(a-a_0(t))^2/2\sigma^2} \tag{S13}$$

with constant $\sigma \ll 1$ and $a_0(t)$ near the fixed point a_{opt}.

Plugging (S13) into the continuity equation (S2), and solving for the highest order (fastest) dynamics of a_0, we see

$$\frac{\mathrm{d}a_0}{\mathrm{d}t} = s\gamma|a-a_0|^{\gamma-1} + 2(1-s)\,(a_{\text{opt}} - a). \tag{S14}$$

Note that (S14) is only true if $\sigma \to 0^+$ faster than $a \to a_0$. If we instead assume $\sigma \to 0^+$ slower than $a \to a_0$, the right-hand side of (S14) is unbounded, and therefore inconsistent with the discrete model. Taking $a \to a_0$ in (S14), we see as expected

$$\frac{\mathrm{d}a_0}{\mathrm{d}t} = 2(1-s)\,(a_{\text{opt}} - a_0).$$

As we see that σ shrinks to 0 faster than $a \to a_0$, we investigate the dynamics of $\sigma(t) \ll 1$ for $a_0 = a_{\text{opt}}$. Again, we take $p(a,t)$ to be a narrow Gaussian distribution

$$p(a,t) = \frac{1}{\sigma(t)\sqrt{2\pi}} e^{-(a-a_0)^2/2\sigma(t)^2}. \tag{S15}$$

Substituting (S15) into (S2) and Taylor expanding about $\sigma = 0$ gives

$$\frac{\mathrm{d}\sigma}{\mathrm{d}t} = \left[\frac{\gamma\,|a-a_0|^{\gamma-1}}{a-a_0} + 2\frac{1-s}{s}\frac{a_{\text{opt}}-a}{a-a_0}\right]\sigma + \mathcal{O}(\sigma^3).$$

We see that as $a \to a_0 = a_{\text{opt}}$ for $\gamma < 2$, the uniform fixed point is unstable (coefficient of σ is ∞). For $\gamma > 2$, the fixed point is stable (coefficient of σ is $-2\frac{1-s}{s}$). The fixed point for $\gamma = 2$ is conditionally stable (coefficient of σ is $\pm 2 - 2\frac{1-s}{s}$). These results agree with the finite N model.

B. Continuum limit two-morph steady state

Next, we investigate the stability of the two-morph steady state. Similar to our investigation of the uniform steady state, we "perturb" the two-morph steady state to the weighted sum of two narrow Gaussian distributions

$$p(a,t) = \frac{x}{\sigma_1(t)\sqrt{2\pi}} e^{-(a-a_1)^2/2\sigma_1(t)^2} + \frac{1-x}{\sigma_2(t)\sqrt{2\pi}} e^{-(a-a_2)^2/2\sigma_2(t)^2}, \tag{S16}$$

where a_1 and a_2 are given by the two-morph fixed point (8). Figure S3 (c),(d) illustrate this idea.

Plugging (S16) into the continuity equation (S2) and using $\bar{a} = xa_1 + (1-x)a_2$, we get a system of two ordinary differential equations for the evolution of σ_1 and σ_2:

$$\begin{aligned} \frac{\mathrm{d}\sigma_1}{\mathrm{d}t} &= \lambda_1\sigma_1 + \mathcal{O}(\sigma_1^3) \\ \frac{\mathrm{d}\sigma_2}{\mathrm{d}t} &= \lambda_2\sigma_2 + \mathcal{O}(\sigma_2^3), \end{aligned} \tag{S17}$$

where λ_1 and λ_2 depend on a_{opt}, s, x, and γ (expressions omitted due to length). Setting $a_{\text{opt}} = 1$ and $s = 1/2$ for instance, we plot the stability region (i.e., where $\lambda_1, \lambda_2 < 0$) for the two-morph steady state in terms of social sensitivity γ and the proportion of males in the large-ornamented group. See figure 3 (d). This is the same stability region we found numerically, which resolves the apparent discrepancy we saw when perturbing the locations of the peaks, but not the widths of the peaks of the two-morph steady state distribution. We have confirmed numerically that convergence to the two-morph fixed points is approximately exponential.

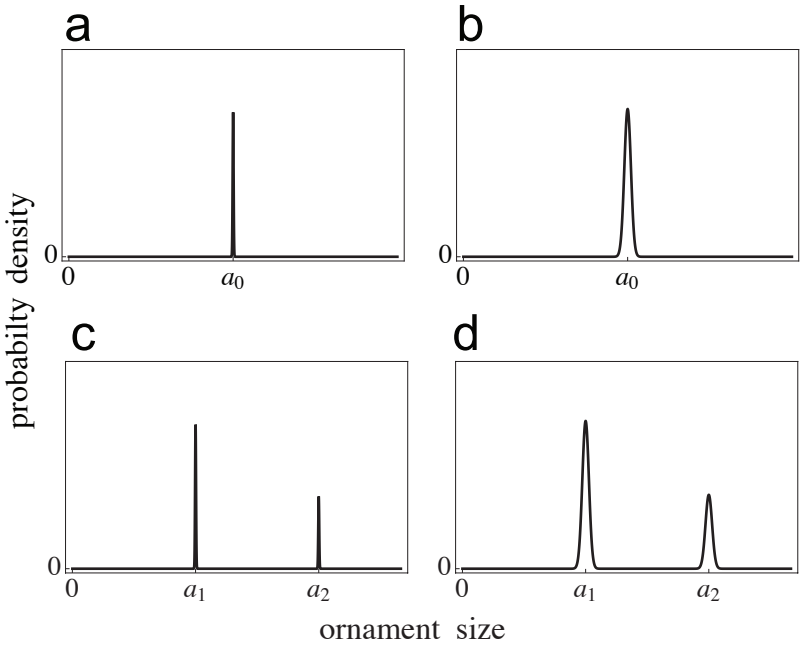

FIG. S3. We consider perturbations to the uniform fixed point $a = a_{\text{opt}}$ and the two-morph fixed point in equation (8) such that the peaks of the distribution are centred at the fixed point solution, and the widths of the peaks are nearly 0. **(a)** Shift peak of the delta uniform solution to a_0. **(b)** Perturb peak width of the delta uniform solution. **(c)** Two-morph steady state. **(d)** Perturb peak widths of the delta two-morph solution.

V. EIGENVALUES OF SYSTEM AS $N \to \infty$

When investigating the stability of the two morph steady state, we chose to take the continuum limit of the model and then investigate the dynamics of the standard deviation of a Gaussian perturbation to the two morph equilibrium. Now we look at the eigenvalues of the finite N system in the limit $N \to \infty$.

Scaling time such that $c = 1$, the Jacobian for the system (5) has diagonal elements

$$J_{ii} = s\gamma(\gamma-1)\left(1-\frac{1}{N}\right)^2 \operatorname{sgn}(a_i-\bar{a})|a_i-\bar{a}|^{\gamma-2} - 2(1-s),$$

and off-diagonal elements

$$J_{ij} = s\gamma(\gamma-1)\left(-\frac{1}{N}\right)\left(1-\frac{1}{N}\right)\operatorname{sgn}(a_i-\bar{a})|a_i-\bar{a}|^{\gamma-2}.$$

As $N \to \infty$,

$$\begin{aligned} J_{ii} &\to s\gamma(\gamma-1)\operatorname{sgn}(a_i-\bar{a})|a_i-\bar{a}|^{\gamma-2} - 2(1-s) \\ J_{ij} &\to 0, \end{aligned}$$

indicating that for large N, the Jacobian matrix is approximately diagonal. Therefore, the diagonal elements are approximately the eigenvalues. Plugging in the two morph fixed point (8), we get two eigenvalues λ_1 and λ_2 with multiplicity xN and $(1-x)N$ respectively. If we plot the stability region (i.e. where $\lambda_1, \lambda_2 < 0$), we see that it's the same as that of the continuum model seen in figure 3 (d).

VI. ALTERNATIVE MULTIPLICATIVE FORM FOR POTENTIAL

Rather than using a weighted sum to construct a total potential as in equation (3) of our main text, we could have considered a weighted product as advocated in [3] and [4], where the authors argue that viability and mating success contribute multiplicatively. We chose to present the mathematical analysis in the context of an additive reproductive

potential because of the greater simplicity, but a multiplicative potential produces the same qualitative results, and can even be considered in the same way by re-interpreting quantities in question on a logarithmic scale (in which case multiplicative terms become additive).

Still, it may be of interest to some readers to see how an explicitly multiplicative model plays out. To create such a model, we first need to scale the reproductive potential functions such that $\varphi^{(\mathrm{soc})}, \varphi^{(\mathrm{ind})} \in [0,1]$ and $a \in [0,1]$.

To retain a quadratic individual potential function with maximum $\varphi^{(\mathrm{ind})} = 1$ and roots at $a = \{0,1\}$, we can choose

$$\varphi^{(\mathrm{ind})} = 4a(1-a), \quad a \in [0,1]. \tag{S18}$$

Note that this choice implies $a_{\mathrm{opt}} = 1/2$[1]. Next, to retain the monotonically increasing social potential function tuned with the social sensitivity γ, we set

$$\varphi^{(\mathrm{soc})} = \frac{\operatorname{sgn}(a-\bar{a})|a-\bar{a}|^{\gamma} + \bar{a}^{\gamma}}{(1-\bar{a})^{\gamma} + \bar{a}^{\gamma}}, \quad a \in [0,1]. \tag{S19}$$

Assuming a weighted product of the individual and social potential terms, the total reproductive potential becomes

$$\varphi = \left(\varphi^{(\mathrm{soc})}\right)^{s} \left(\varphi^{(\mathrm{ind})}\right)^{1-s}, \tag{S20}$$

where $\varphi^{(\mathrm{soc})}$ and $\varphi^{(\mathrm{ind})}$ are (S19) and (S18), respectively, and s tunes the relative importance of each term. Plugging this into equation (4) of the main text, we get

$$\frac{\mathrm{d}a}{\mathrm{d}t} = c\left[s\left(\frac{\varphi^{(\mathrm{ind})}}{\varphi^{(\mathrm{soc})}}\right)^{1-s} \frac{\partial}{\partial a}\varphi^{(\mathrm{soc})} + (1-s)\left(\frac{\varphi^{(\mathrm{ind})}}{\varphi^{(\mathrm{soc})}}\right)^{-s} \frac{\partial}{\partial a}\varphi^{(\mathrm{ind})}\right] \tag{S21}$$

or

$$\frac{\mathrm{d}a}{\mathrm{d}t} = c\left(\frac{\varphi^{(\mathrm{ind})}}{\varphi^{(\mathrm{soc})}}\right)^{-s}\left[s\left(\frac{\varphi^{(\mathrm{ind})}}{\varphi^{(\mathrm{soc})}}\right)\frac{\partial}{\partial a}\varphi^{(\mathrm{soc})} + (1-s)\frac{\partial}{\partial a}\varphi^{(\mathrm{ind})}\right]. \tag{S22}$$

We observe that (S22) retains the form of a weighted sum of two terms, though the split of natural and sexually selective forces is now more complicated. The weights are different from (5), but remain positive, and the general arguments for existence of multimodal equilibrium distributions may be extended to this system in a straightforward way.

VII. MECHANISMS FOR BIMODALITY

A key feature of our model is that it is agnostic to the genetic mechanism by which the two-morph distribution is maintained. That is, we make no assumptions about the genetics other than presuming that maintenance of such a distribution is possible (by some mechanism). Rather, we demonstrate that the bimodal distribution—and thus a mechanism to maintain it—is an emergent, evolutionarily favorable consequence of Zahavi's handicap principle.

There are several molecular mechanisms by which a population with multiple optima can be maintained, including overdominance, complex polygenic or epistatic relationships, or epigenetic modifications. Any of these (amongst others) could be involved in the maintenance of the predicted bimorphic trait. Because our model makes no assumptions (or predictions) about which of these mechanisms maintain the two-morph state, it is general to any organismal trait where Zahavi's handicap principle applies, and is insensitive to assumptions about the genetic architecture.

Of course, we do not wish to imply that our model is the only possible explanation (or even necessarily the dominant effect) where polymorphism is observed. The importance of this effect probably varies from species to species and ornament to ornament.

VIII. APPLICABILITY OF MODEL

Our model applies most naturally to inter-sexual selection (female choice as the dominating force), and in the interest of simplicity we ignore alternative reproductive strategies (e.g., female mimicry by males). We believe that it may be possible to generalize our model to include effects like negative-frequency dependent selection—e.g., as another type of social effect that would impact the shape of the social potential function in our model—but leave that for future work.

---

[1] A more general form allowing for arbitrary a_{opt} would map $a \to a^{\alpha}$, where $\alpha = -\ln(2)/\ln(a_{\mathrm{opt}})$.

IX. STATISTICAL ANALYSIS OF ORNAMENTATION DATA

Our model for the evolution of costly mating displays predicts the emergence of two distinct morphs of ornament sizes. We tested whether the two-morph state was detectable in a variety of ornament datasets (figures S5,S6). Three approaches were used: a parametric mixture–model fit; the nonparametric but highly conservative Hartigans' Dip Test for bimodality [5]; and a simulation–based nonparametric test which improves upon the Hartigan test sensitivity.

We present test results for Hartigans' Dip Test and the simulation–based nonparametric test, called the LUU (Least Unimodal Unimodal) test for reasons that will be clear, in table I. Test results for the parametric–model fit are in table II.

A. Parametric two-morph test

All count and size measurement data were log-transformed prior to analysis (as is typical for physical measurements) to account for the bounded support of size distributions. Here, we make the assumption that ornament sizes within a morph will be log-normally distributed, and that a multi-morph state will exhibit a mixture of distributions. We thus fit Gaussian mixture models with 1–5 components of unequal variance to the log-transformed data and find the number of components that yields the best BIC [6]. In the absence of a social fitness pressure, we expect the best fit to be a single Gaussian (corresponding to the one morph state), while the two–morph state predicted from our model will have the best fit with ≥ 2 components.

B. Hartigans' dip test

An essential drawback of using the above mixture model fit to assess the number of ornament–size morphs in the data is that it is extremely sensitive to deviations from the parametric assumption that a one–morph state will be well–described by a single Gaussian. False positives are likely when those assumptions are violated; if a single–morph state has a skewed (or otherwise non-normal) distribution, a mixture of ≥ 2 Gaussians will generally give a higher BIC than a single–component distribution.

A more conservative approach is to look for evidence of strict multimodality (with dips in the distribution), rather than a mixture (which may not exhibit a "dip"). Hartigan and Hartigan define the dip statistic D as the maximum difference between the empirical cumulative distribution function and the CDF of the unimodal distribution that minimises that maximum difference. The reference distribution is customarily taken to be the uniform distribution, the least singly–peaked of all unimodal distributions. The p-value for the dip is calculated by comparing D to those obtained from repeated samples of the same size drawn from a uniform distribution. The dip test thus measures whether the empirical distribution of the data exhibits greater departure from unimodality than would be expected from a sample of the same size if the underlying distribution were uniform.

C. Bootstrap dip test

While the mixture test may be overly sensitive in detecting deviations from a single morph, Hartigans' dip test is likely to be excessively conservative and insensitive at small sample sizes. A finite sample drawn from a uniform distribution will, with high probability, have a larger dip by chance than a finite sample drawn from a two–morph distribution such as those shown in figure 4 (a),(b).

To address this problem, we propose a bootstrap dip test which takes as its reference distribution the "least unimodal" unimodal density estimate of the sample. Given a finite sample, we construct a kernel density estimate (KDE) using a Gaussian kernel at various bandwidths. At very large bandwidths, the KDE will be unimodal; as the bandwidth is reduced, the KDE will approach a multimodal distribution with as many modes as there are unique values in the dataset. We define the least–unimodal unimodal (LUU) distribution to be that obtained from the smallest bandwidth for which the KDE is still strictly unimodal.

From this LUU density estimate, we generate random samples of the same size as the original data, and compute their dip statistics. These bootstrapped samples serve as the reference distribution against which the dip statistic of the data is compared. This test thus measures whether the empirical distribution of the data exhibits greater departure from unimodality than would be expected from a sample of the same size if the underlying distribution were *the unimodal distribution best fit to the sample*. Figure S4 illustrates that this bootstrap dip test is more sensitive to bimodality than Hartigans' Dip Test.

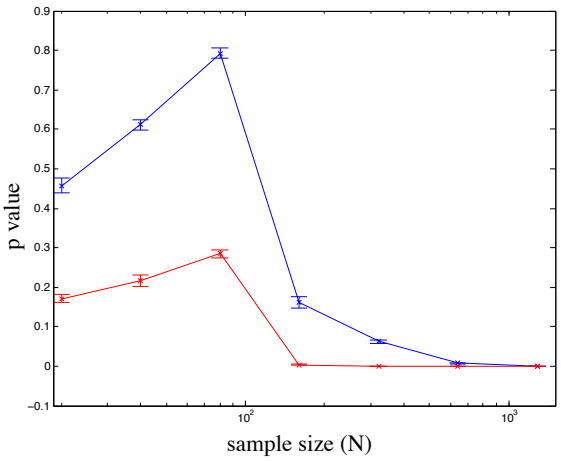

FIG. S4. For small sample sizes of bimodal data, like we have for most of our animal data sets, the p-values for bimodality using Hartigans' Dip Test (blue) are larger than our bootstrap dip test (red). As the sample size increases, we gain significance using our test first and Hartigans' Dip Test eventually, showing our test is less conservative. The data used here are equilibrium states of our model (5) for $\gamma = 1.5, s = 0.5$, and a_{opt} drawn from a normal distribution with mean 1 and standard deviation 0.25. We know these samples are bimodal. Error bars are standard deviations from 10 trials.

X. ADDITIONAL DATA AND ANALYSIS

We have additional data sets of ornament distribution from various species in figures S5 and S6. The kernel density curves are superimposed for reference. If body size is a form of advertising, then we may also use data of salmon [25], trout [26], wolf spiders [27], and other bimodally distributed species. See figure S7.

While this work is based on mating displays in the animal kingdom, we hypothesise that similar forces operate on plants that compete within their own species for resources. For instance, a tree's height could be analogous to ornament size in our model, in that growing taller incurs costs to the individual, but being relatively taller in a forest has competitive benefits. In fact, certain tree species exhibit bimodal height distributions [28, 29]. See figure S8.

XI. CONNECTION TO SPECIATION MODELS

We speculate that the mechanism we describe here may also have implications for speciation. Models of speciation presented in Lande [4] and Stewart [31] are similar to our ornamentation model in both form and outcome. Stewart claims that for an all-to-all system of behaviourally identical individuals (like ours), the population will split into two species for most environmental conditions. Like our social sensitivity γ, Stewart's environmental factor λ varies on a slow time scale relative to the dynamical system. Also like our model, Stewart's model exhibits similar fractionation (simulating 100 individuals, the population splits into "clumps" of 84 and 16).

Lande uses quantitative genetics techniques to show that sexual selection may lead to speciation. Our model is quite similar to Lande's model interpreted on a logarithmic scale. Like our model, Lande's sexual selection alone would lead to runaway ornament sizes, but natural selection stabilises growth. Unlike our model, Lande states that "natural selection on mating preferences also creates the possibility of evolutionary oscillations." Because we ignore the long time scale effects of female choice, our model precludes the possibility of oscillations.

Data set	N	p-value (Dip test)	p-value (LUU test)	p-value (Dip test - log data)	p-value (LUU test - log data)	Tests reject unimodality?
Dung beetle horn length (Emlen [7])	223	0.0011**	0.0001***	0.0035**	0.0000***	yes
Yellow-breasted chat plumage coloration (Mays [8])	62	0.1932	0.0530	0.5479	0.2652	no
Peacock eye spots (Loyau [9])	24	0.6390	0.3793	0.5965	0.3187	no
Peacock eye spots (Petrie [10])	24	0.9183	0.7682	0.8809	0.6963	no
Peacock eye spots (Loyau/Petrie merged)	48	0.9016	0.6699	0.9006	0.6587	no
Arctic charr skin brightness (Skarstein [11])	20	0.2633	0.1558	0.2802	0.1658	no
Salmon body size (Glover [12])	72	0.6206	0.1467	0.7432	0.2497	no
Widowbird tail length (Anderson [13])	107	0.9992	0.9700	0.9972	0.9594	no
Widowbird red collar patch size (Anderson [13])	107	0.0046**	0.0002***	0.0317*	0.0030**	yes
Barn owl spottiness (Nieche [14])	20	0.6476	0.3858	0.7196	0.5157	no
Finch carotenoid coloration (Badyaev [15])	68	0.5295	0.1927	NA	NA	no
Stickleback nest compactness (Barber [16])	38	0.6085	0.2221	NA	NA	no
Partridge black ventral area (Bortolotti [17])	29	0.9032	0.6652	0.8704	0.5812	no
Roe deer antler length (Pelabon [18])	242	0.0341*	0.0012**	0.0232*	0.0001***	yes
Lion >2.2 yrs mane length (West [19])	441	0.8687	0.4134	0.9873	0.9521	no
Lion >2.2 yrs mane darkness (West [19])	442	0.9078	0.6698	0.9602	0.9033	no
Lion >5 yrs mane length (West [19])	257	0.8085	0.4779	0.8557	0.5356	no
Lion >5 yrs mane darkness (West [19])	257	0.8285	0.4129	0.8567	0.5173	no
Dung beetle horn length - WA (Moczek [20])	644	0.0000***	0.0000***	0.0000***	0.0000***	yes
Dung beetle horn length - NC (Moczek [20])	1016	0.0000***	0.0000***	0.0000***	0.0000***	yes
Earwig forceps length (Tomkins [21])	134	0.0000***	0.0000***	0.0000***	0.0000***	yes
Great tit stripe length (Norris [22])	63	0.2034	0.0781	NA	NA	no
Fiddler crab fight duration (Hyatt [23])	80	0.7059	0.2601	0.6362	0.3312	no
Fiddler crab fight acts (Hyatt [23])	80	0.8966	0.5273	0.9006	0.5714	no

TABLE I. Unimodality test results for animal ornamentation data sets. Hartigans' Dip Test (Dip test) is more conservative than our bootstrap dip test (LUU test); therefore our LUU test is more likely to reject unimodality. We performed both tests on log-transformed data because tissue measurements are often log-normally distributed [24]. We note in the rightmost column if the unimodality tests reject the null hypothesis that the distributions of ornament size are unimodal. Note that we exclude p-values for log-transformed data (NA) if the original data is not a straight-forward measurement of tissue investment.

Data set	N	fractionation	morph means	morph variances	fractionation (log data)	morph means (log data)	morph variances (log data)
Dung beetle horn length (Emlen [7])	223	0.2372 0.2677 0.2414 0.2156 0.0380	0.2631 1.0576 0.7280 0.1204 0.5126	0.0055 0.0112 0.0142 0.0018 0.0000	0.0448 0.2103 0.3299 0.1950 0.2200	-2.8934 -1.3094 -0.3286 -2.0101 0.0629	0.0005 0.0509 0.0553 0.0412 0.0082
Yellow-breasted chat plumage coloration (Mays [8])	62	0.7247 0.2753	40.2987 23.7743	58.3743 4.9154	0.2924 0.7076	3.1794 3.6963	0.0084 0.0302
Peacock eye spots (Loyau [9])	24	1.0000	152.0645	46.7236	1.0000	5.0233	0.0021
Peacock eye spots (Petrie [10])	24	1.0000	145.9515	95.9004	1.0000	4.981	0.0046
Peacock eye spots (Loyau/Petrie merged)	48	1.0000	149.0080	80.6543	1.0000	5.0021	0.0038
Arctic charr skin brightness (Skarstein [11])	20	0.4505 0.5495	2.3538 2.5160	0.0015 0.0004	0.4507 0.5493	0.8559 0.9226	0.0003 0.0001
Salmon body size (Glover [12])	72	0.1383 0.8617	9.3169 14.6375	0.5107 1.0055	0.1388 0.8612	2.2296 2.6814	0.0056 0.0046
Widowbird tail length (Anderson [13])	107	1.0000	221.5356	796.5005	1.0000	5.3920	0.0179
Widowbird red collar patch size (Anderson [13])	107	1.0000	222.1704	2419.6	1.0000	5.3779	0.0526
Barn owl spottiness (Nieche [14])	20	1.0000	1.2436	0.4555	1.0000	0.0695	0.3068
Finch carotenoid coloration (Badyaev [15])	68	1.0000	1.7732	3.1678	NA	NA	NA
Stickleback nest compactness (Barber [16])	38	0.8947 0.1053	37.7314 90.2335	99.9319 0.0131	NA	NA	NA
Partridge black ventral area (Bortolotti [17])	29	1.0000	21.1812	56.7020	1.0000	2.9779	0.1728
Roe deer antler length (Pelabon [18])	242	0.0903 0.9097	12.1801 18.1135	7.7178 5.1123	0.1235 0.8765	2.5521 2.8933	0.0693 0.0144
Lion > 2.2 yrs mane length (West [19])	442	0.1936 0.8064	0.6800 1.2663	0.0192 0.0338	0.7171 0.2829	0.2489 -0.2681	0.0166 0.0827
Lion > 2.2 yrs mane darkness (West [19])	442	1.0000	1.1008	0.0562	0.6464 0.3536	0.1695 -0.1118	0.0217 0.0673
Lion> 5 yrs mane length (West [19])	257	1.0000	1.2977	0.0319	0.0383 0.9617	-0.1331 0.2652	0.0814 0.0145
Lion > 5 yrs mane darkness (West [19])	257	1.0000	1.2021	0.0363	0.3205 0.6795	0.0484 0.2283	0.0351 0.0142
Dung beetle horn length - WA (Moczek [20])	644	0.3546 0.0837 0.1616 0.1910 0.2091	0.5105 2.0758 1.1310 0.6517 3.9032	0.0033 0.4042 0.0782 0.0110 0.2139	0.4784 0.2111 0.3105	-0.6237 1.3512 0.1371	0.0224 0.0152 0.2152
Dung beetle horn length - NC (Moczek [20])	1016	0.2301 0.1633 0.2268 0.3799	2.6811 0.9594 0.5430 4.0161	0.6706 0.0686 0.0097 0.1330	0.2423 0.1907 0.2292 0.3378	0.1279 1.1523 -0.6075 1.4015	0.2082 0.0295 0.0418 0.0064
Earwig forceps length (Tomkins [21])	134	0.3165 0.2501 0.4333	5.9727 7.3120 3.5705	0.7099 0.1154 0.0982	0.2964 0.2460 0.4576	1.8033 1.9901 1.2796	0.0144 0.0020 0.0098
Great tit stripe length (Norris [22])	63	0.5789 0.4211	-14.1532 17.1432	77.5214 60.9468	NA	NA	NA
Fiddler crab fight duration (Hyatt [23])	80	0.0500 0.4433 0.1848 0.3219	482.1489 19.5720 51.5698 125.9917	5555.8303 65.1629 33.6134 2189.0050	1.0000	3.8413	1.1077
Fiddler crab fight acts (Hyatt [23])	80	0.1103 0.2370 0.6526	53.5474 26.7320 11.3968	555.7647 14.2841 22.7231	1.0000	2.7213	0.5112

TABLE II. We fit Gaussian mixture models with 1–5 components of unequal variance to the animal ornamentation data sets and find the number of components that yields the best BIC [6]. We performed this fit on log-transformed data because tissue measurements are often log-normally distributed [24]. Note that we exclude Gaussian mixture models for log-transformed data (NA) if the original data is not a straight-forward measurement of tissue investment.

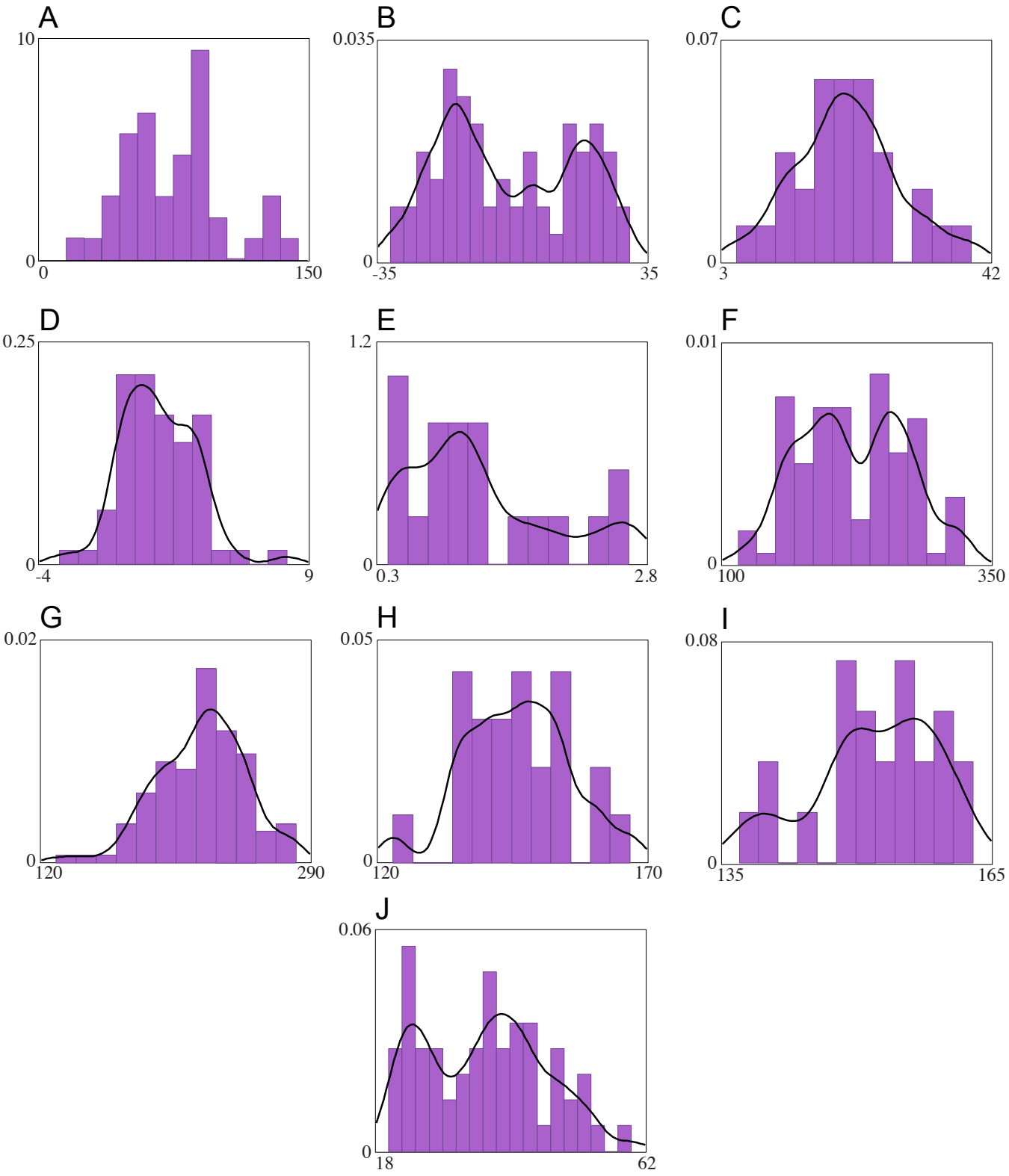

FIG. S5. Additional ornament data sets (birds) **A.** Blackbird song pulse repetition rate [30] (data extracted from histogram, so sample size uncertain) **B.** Great tit stripe size [22] (N=63) **C.** Partridge black ventral area [17] (N=29) **D.** Finch carotenoid coloration [15] (N=68) **E.** Barn owl spottiness [14] (N=20) **F.** Widowbird collar patch size [13] (N=107) **G.** Widowbird tail length [13] (N=107) **H.** Peacock eye spots [10] (N=24) **I.** Peacock eye spots [9] (N=24) **J.** Yellow-breasted chat plumage color [8] (N=62)

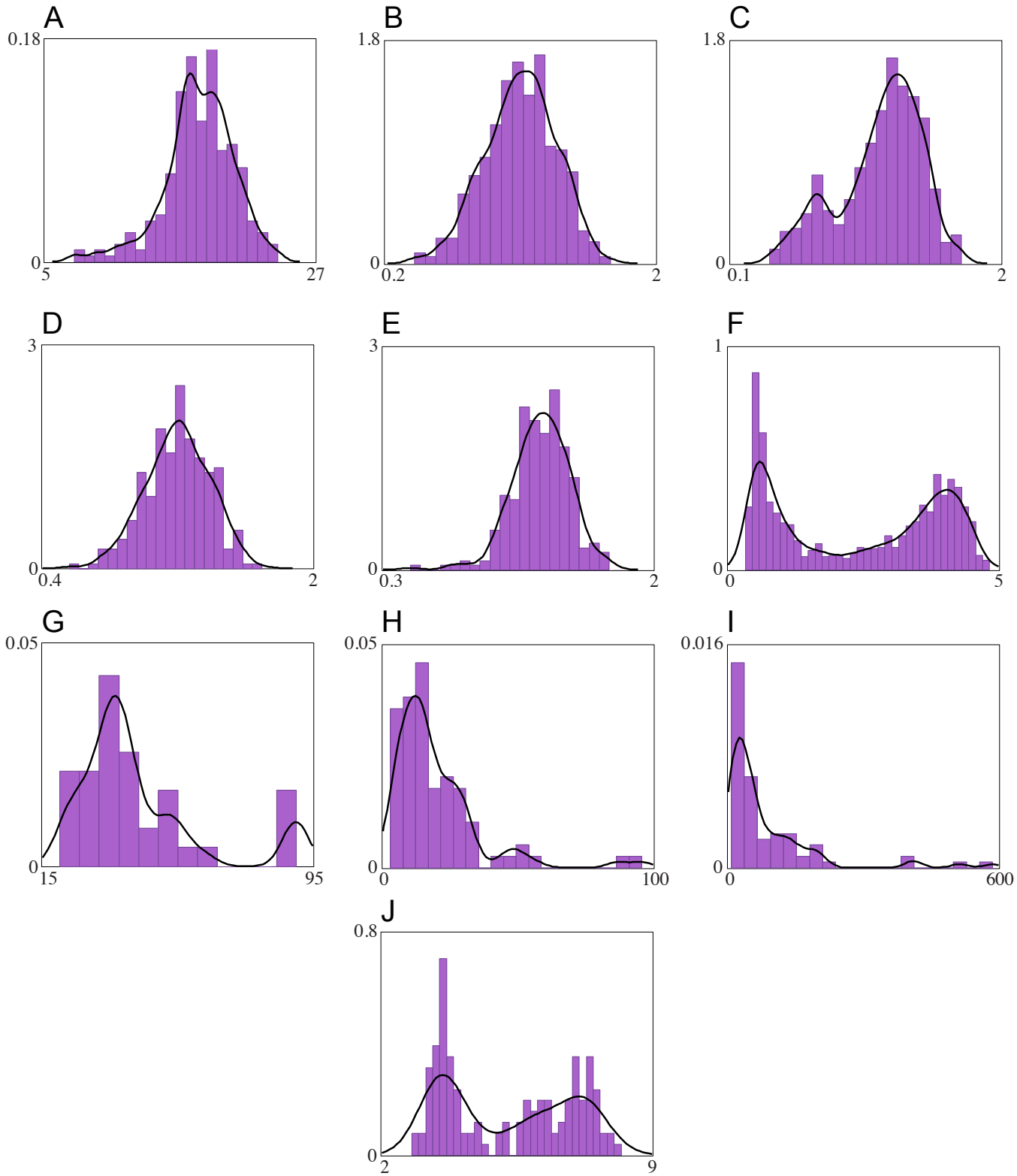

FIG. S6. Additional ornament data sets **A.** Roe deer antler length [18] (N=242) **B.** Mature (> 2.2 yr) lion mane darkness [19] (N=442) **C.** Mature (> 2.2 yr) lion mane length [19] (N=442) **D.** Older (> 5 yr) lion mane darkness [19] (N=257) **E.** Older (> 5 yr) lion mane length [19] (N=257) **F.** Dung beetle horn length (North Carolina) [20] (N=1016) **G.** Stickleback nest compactness [16] (N=38) **H.** Fiddler crab fight acts [23] **I.** Fiddler crab fight duration [23] **J.** Earwig forceps length [21] (N=134)

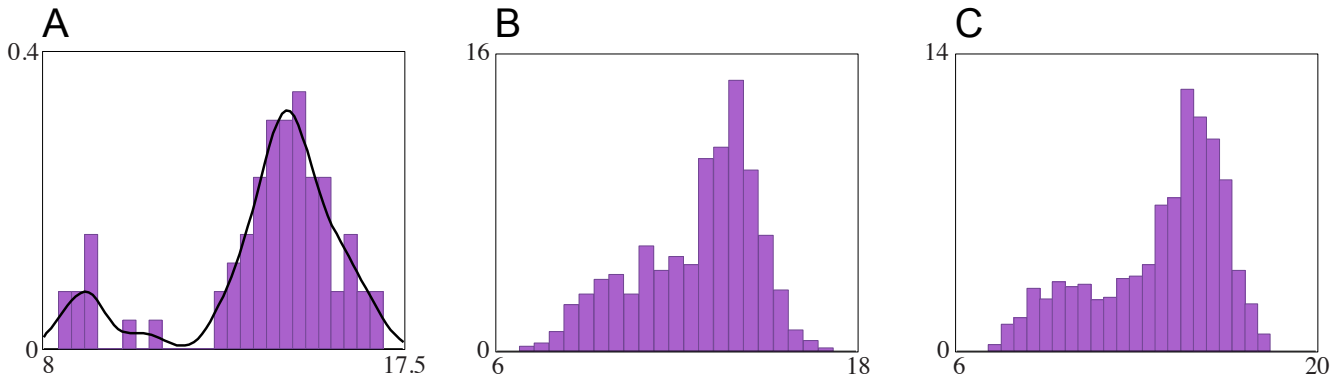

FIG. S7. Bimodal body size data sets **A.** Salmon body size [12] (N=72) **B.** Trout body size (early season) [26] (data extracted from histogram, so sample size uncertain) **C.** Trout body size (late season) [26] (data extracted from histogram, so sample size uncertain)

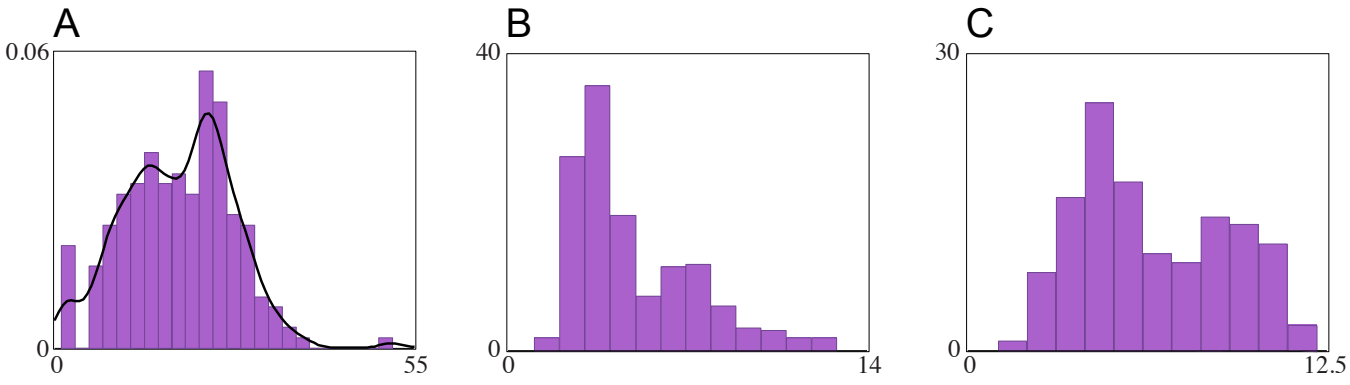

FIG. S8. Bimodal forest data sets **A.** Diameter at breast height for B. platyphylla trees [28] (N=217) **B.** Diameter at breast height for B. ermanii (11-16 yrs old) [29] (data extracted from histogram, so sample size uncertain) **C.** Height of B. ermanii (11-16 yrs old) [29] (data extracted from histogram, so sample size uncertain)

[1] M. A. Nowak, *Evolutionary Dynamics*. Harvard University Press, 2006.

[2] G. P. Karev, "On mathematical theory of selection: continuous time population dynamics," *Journal of mathematical biology*, vol. 60, no. 1, pp. 107–129, 2010.

[3] T. Getty, "Sexually selected signals are not similar to sports handicaps," *Trends in Ecology & Evolution*, vol. 21, no. 2, pp. 83–88, 2006.

[4] R. Lande, "Models of speciation by sexual selection on polygenic traits," *Proceedings of the National Academy of Sciences*, vol. 78, no. 6, part 2, pp. 3721–3725, 1981.

[5] J. A. Hartigan and P. M. Hartigan, "The dip test of unimodality," *The Annals of Statistics*, vol. 13, no. 1, pp. 70–84, 1985.

[6] G. Schwarz, "Estimating the dimension of a model," *The Annals of Statistics*, vol. 6, no. 2, pp. 461–464, 1978.

[7] D. J. Emlen, "Artificial selection on horn length-body size allometry in the horned beetle Onthophagus acuminatus (Coleoptera: Scarabaeidae)," *Evolution*, vol. 50, no. 3, pp. 1219–1230, 1996.

[8] H. L. Mays, Jr, K. J. McGraw, G. Ritchison, S. Cooper, V. Rush, and R. S. Parker, "Sexual dichromatism in the yellow-breasted chat Icteria virens: spectrophotometric analysis and biochemical basis," *Journal of Avian Biology*, vol. 35, no. 2, pp. 125–134, 2004.

[9] A. Loyau, M. Saint Jalme, C. Cagniant, and G. Sorci, "Multiple sexual advertisements honestly reflect health status in peacocks (Pavo cristatus)," *Behavioral Ecology and Sociobiology*, vol. 58, no. 6, pp. 552–557, 2005.

[10] M. Petrie and T. Halliday, "Experimental and natural changes in the peacock's (Pavo cristatus) train can affect mating success," *Behavioral Ecology and Sociobiology*, vol. 35, no. 3, pp. 213–217, 1994.

[11] F. Skarstein and I. Folstad, "Sexual dichromatism and the immunocompetence handicap: an observational approach using arctic charr," *Oikos*, vol. 76, pp. 359–367, 1996.

[12] K. A. Glover, C. Skår, K. E. Christie, J. Glette, H. Rudra, and Ø. Skaala, "Size-dependent susceptibility to infectious salmon anemia virus (ISAV) in Atlantic salmon (Salmo salar L.) of farm, hybrid and wild parentage," *Aquaculture*, vol. 254, no. 1-4, pp. 82–91, 2006.

[13] S. Andersson, S. R. Pryke, J. Örnborg, M. J. Lawes, and M. Andersson, "Multiple Receivers, Multiple Ornaments, and a Trade-off between Agonistic and Epigamic Signaling in a Widowbird," *The American Naturalist*, vol. 160, no. 5, pp. 683–691, 2002.

[14] M. Niecke, S. Rothlaender, and A. Roulin, "Why do melanin ornaments signal individual quality? Insights from metal element analysis of barn owl feathers," *Oecologia*, vol. 137, no. 1, pp. 153–158, 2003.

[15] A. Badyaev, "Evolution of sexual dichromatism: contribution of carotenoid- versus melanin-based coloration," *Biological journal of the Linnean Society*, vol. 69, no. 2, pp. 153–172, 2000.

[16] I. Barber, D. Nairn, and F. A. Huntingford, "Nests as ornaments: revealing construction by male sticklebacks," *Behavioral Ecology*, vol. 12, no. 4, pp. 390–396, 2001.

[17] G. R. Bortolotti, J. Blas, J. J. Negro, and J. L. Tella, "A complex plumage pattern as an honest social signal," *Animal Behaviour*, vol. 72, no. 2, pp. 423–430, 2006.

[18] C. Pélabon and L. van Breukelen, "Asymmetry in antler size in roe deer (Capreolus capreolus): an index of individual and population conditions," *Oecologia*, vol. 116, no. 1-2, pp. 1–8, 1998.

[19] P. M. West, "Sexual Selection, Temperature, and the Lion's Mane," *Science*, vol. 297, no. 5585, pp. 1339–1343, 2002.

[20] A. P. Moczek and H. F. Nijhout, "Developmental mechanisms of threshold evolution in a polyphenic beetle," *Evolution & Development*, vol. 4, no. 4, pp. 252–264, 2002.

[21] J. L. Tomkins, J. S. Kotiaho, and N. R. LeBas, "Matters of Scale: Positive Allometry and the Evolution of Male Dimorphisms," *The American Naturalist*, vol. 165, no. 3, pp. 389–402, 2005.

[22] K. J. Norris, "Female choice and the quality of parental care in the great tit Parus major," *Behavioral Ecology and Sociobiology*, vol. 27, no. 4, pp. 275–281, 1990.

[23] G. W. Hyatt and M. Salmon, "Combat in the fiddler crabs Uca pugilator and U. pugnax: a quantitative analysis," *Behaviour*, vol. 65, no. 1, pp. 182–211, 1978.

[24] J. S. Huxley, *Problems of Relative Growth*. New York: L. MacVeagh, The Dial Press, 1932.

[25] J. E. Thorpe, "Bimodal distribution of length of juvenile Atlantic salmon (Salmo salar L.) under artificial rearing conditions," *Journal of Fish Biology*, vol. 11, no. 2, pp. 175–184, 1977.

[26] K. A. Glover, O. T. Skilbrei, and Ø. Skaala, "Stock-specific growth and length frequency bimodality in brown trout," *Transactions of the American Fisheries Society*, vol. 132, no. 2, pp. 307–315, 2003.

[27] A. Aisenberg and F. G. Costa, "Reproductive isolation and sex-role reversal in two sympatric sand-dwelling wolf spiders of the genus Allocosa," *Canadian Journal of Zoology*, vol. 86, no. 7, pp. 648–658, 2008.

[28] M. P. Eichhorn, "Spatial organisation of a bimodal forest stand," *Journal of Forest Research*, vol. 15, no. 6, pp. 391–397, 2010.

[29] M. Yokozawa and T. Hara, "Foliage profile, size structure and stem diameter-plant height relationship in crowded plant populations," *Annals of Botany*, vol. 76, no. 3, pp. 271–285, 1995.

[30] W. A. Searcy, "Species recognition of song by female red-winged blackbirds," *Animal Behaviour*, vol. 40, no. 6, pp. 1119–1127, 1990.

[31] I. Stewart, "Speciation: a case study in symmetric bifurcation theory," *Universitatis Iagellonicae Acta Mathematica*, vol. 41, pp. 67–88, 2003.